OFFICE OF NAVAL RESEARCH

Contract No. N00014-91-J-1409

Technical Report No. 125

The Role of Interfacial Potential in Adsorbate Bonding: Electrode Potential-Dependent Infrared Spectra for Saturated CO Adlayers on Pt(110) and Related Electrochemical Surfaces in Varying Solvent Environments

by

X. Jiang and M.J. Weaver

Prepared for Publication

in

Surface Science

Purdue University

Department of Chemistry

West Lafayette, Indiana 47907

May 1992

ABSTRACT

Infrared spectra in the C–O stretching (ν_{co}) region are reported for saturated CO adlayers on Pt(110) in various solvent media over wide (ca 3 V) ranges of electrode potential in order to explore the influence of the surface potential in various ionic double-layer environments on the adsorbate bonding. The solvents chosen – acetonitrile, tetrahydrofuran, dichloromethane, methanol, and water – span a wide range of polarity and other properties. The double-layer cations, constituting the ionic countercharge to the negative surface electronic charges encountered here, were tetrabutylammonium (TBA^+), tetraethylammonium (TEA^+) and sodium, present as the perchlorate salts. The tetraalkylammonium ions provide noninteracting cations of differing size, enabling the effects of altering the inner-layer thickness to be examined. In such media, a single terminal ν_{co} feature (referring to a coverage $\theta_{co} \approx 1.0$) is obtained on Pt(110) throughout the potential range ca –2 to 1 V vs aqueous saturated calomel electrode (SCE), with frequencies (ν_{co}^t) in the range 2050–2100 cm^{-1}, decreasing linearly with potential (E). While the ν_{co}^t–E behavior is approximately independent of the solvent, the slopes observed in TEA^+ (20–21 cm^{-1} V^{-1}) are significantly greater than in TBA^+ (15–17 cm^{-1} V^{-1}). These differences can be interpreted by using a simple double-layer model where the inner-layer thickness is determined by the CO adlayer plus the cation crystallographic radius (cf refs. 8,11). The potential of zero charge, $E_{pzc} \approx 0.8$ V vs SCE, as determined by the intersection point of these ν_{co}^t–E plots is consistent with the surface potential of the (necessarily uncharged) Pt(110)/CO interface in ultrahigh vacuum (uhv) as determined by work-function measurements. Similar findings were obtained for saturated CO adlayers on Rh(111), although bridging as well as terminal CO coordination is observed and a potential-induced site conversion is obtained in some solvating environments. In acetonitrile with sodium perchlorate electrolyte, terminal to bridging site conversion was induced at all three surfaces at increasingly negative electrode potentials in the sequence Pt(110) < Pt(111) < Rh(111); such effects arise apparently from specific Na^+–CO adlayer interactions. The dependencies of the ν_{co} frequencies on the potential drop across the CO adlayer as deduced here are compared with related results obtained for Pt(111)/CO in uhv.

INTRODUCTION

The surface potential, together with the accompanying electrostatic fields, have long been recognized by electrochemists as playing a central role in the properties of adsorbates at metal–solution interfaces. This appreciation has arisen in large part through the ease by which the surface potential in electrochemical systems (as controlled by the electrode potential) can be varied by external means. Similar potential–induced effects can be anticipated to also play a role in adsorbate properties at metal–ultrahigh vacuum (uhv) interfaces, especially in the presence of dipolar or ionizable coadsorbates.[1,2] The recognition as well as understanding of such effects in the latter case, however, has been hampered somewhat by the more limited control of the surface potential attainable in uhv systems, together with the relative paucity of the required work–function data. Even so, some intriguing information on potential–induced effects upon the thermodynamic and spectroscopic adsorbate properties in uhv environments has been obtained by dosing components of electrochemical interfaces at metal–uhv surfaces.[1]

An alternative, yet complementary, approach to exploring such factors entails obtaining potential–dependent molecular spectroscopic information for adsorbates at in–situ electrochemical surfaces. A particularly suitable technique for this purpose is infrared reflection–absorption spectroscopy (IRAS). While most applications of IRAS to in–situ electrochemical interfaces have utilized polycrystalline metals, an increasing number of studies are focussing on ordered monocrystalline surfaces.[2] A further close connection with metal–uhv systems has been forged by employing carbon monoxide as a probe adsorbate.[2]

So far, almost all IRAS studies of this type from our laboratory and elsewhere have involved metal–aqueous solution interfaces (refs. 2–7 are representative). Despite the importance and convenience of water as a solvent, an obvious restriction is that the range of electrode potentials that can be

accessed is limited severely by cathodic hydrogen evolution and CO electrooxidation. In a recent preliminary communication, we have reported potential-dependent infrared spectra for saturated CO adlayers on ordered Pt(111) in several nonaqueous solvents: acetonitrile, dimethylformamide, dichloromethane, and tetrahydrofuran (THF), containing tetraalkylammonium perchlorate electrolytes.[8] These systems enable the C–O adsorbate vibrational (ν_{CO}) bands to be examined over wide (up to ca 3.5 V) ranges of electrode potential, encompassing surface potentials appropriate to analogous metal–uhv interfaces. Notably, the spectral features, especially the ν_{CO} frequencies and CO site occupancies, were found to be sensitive only to the applied potential, being virtually independent of the solvating medium in the presence of a given electrolyte cation.[8] These results, along with the observed dependence of the ν_{CO} frequency–potential data on the cation size and comparisons with spectra for corresponding Pt(111)–aqueous and uhv interfaces, demonstrate that the CO adlayer properties are controlled in each case chiefly by the surface-potential drop across the adsorbate layer.

In view of these surprisingly straightforward findings for Pt(111), it is of interest to expand such explorations of CO adlayer properties to embrace other monocrystalline surfaces. Our recent IRAS studies of low-index platinum– and rhodium–aqueous interfaces[2–5] prompted us to examine in particular Pt(110) and Rh(111). The former surface, unlike Pt(111), has the distinctive feature of maintaining exclusively terminal (i.e., atop) CO coordination over wide ranges of electrode potential.[3c,5] This unusual property simplifies the examination of ν_{CO} frequency–potential relationships since accompanying variations in the binding-site occupancy should be essentially absent, at least in the absence of specific cation effects (vide infra). The Rh(111)/CO–aqueous interface, on the other hand, exhibits a transition from largely terminal to twofold bridging CO coordination for potentials below ca 0 V vs the saturated calomel electrode (SCE).[5,9] This potential-induced site conversion is the most dramatic example

of the progressive shift towards multifold CO coordination at lower potentials commonly observed at low-index platinum and rhodium electrode surfaces.[2,5] Given that the CO site conversion on Pt(111) is observed to be largely unaffected by the solvent medium,[8] it is of interest to ascertain if the more marked potential-dependent behavior on Rh(111) is similarly unaffected by the solvation as well as the ionic environment. Additional comparative results on Pt(111) are also reported here.

The solvents selected for examination – acetonitrile, THF, dichloromethane, methanol, and water – span a wide range of polarity and related properties. As before, tetrabutylammonium and tetraethylammonium perchlorates were employed as supporting electrolytes so to provide a pair of noninteracting double-layer cations of differing size. While the use of a wider range of tetraalkylammonium salts was thwarted by solubility limitations, these cations enable the effect of varying the inner-layer thickness, and hence the field across the CO adlayer at a given electrode potential, to be explored.[10,11] Sodium perchlorate electrolyte was additionally examined, since it provides an example of a more specifically interacting cation known to engender potential-induced CO site conversion in some cases.[10,11]

EXPERIMENTAL

Details of the electrochemical IRAS measurements are largely as provided in refs. 12 and 13. The infrared spectrometer was an IBM (Bruker) IR-98-4A Fourier transform instrument, with a Globar light source and a liquid-N_2 cooled MCT detector (Infrared Associates). The spectral resolution was usually ± 4 cm^{-1}.

The low-index Pt and Rh faces (0.9-1.0 cm diameter, 2-4 mm thick) were purchased from the Materials Preparation Facility at Cornell University. They were oriented within $\pm 1°$, as verified by X-ray diffraction. The surface pretreatment procedures, including hydrogen-air flame annealing, gas-phase iodine adsorption during cooling, and subsequent replacement with adsorbed CO in aqueous solutions, were adapted from those of Wieckowski and coworkers,[14] as detailed in

ref. 15 for Pt and ref. 16 for Rh surfaces. After removal of the irreversibly adsorbed CO by a positive-going voltammetric sweep, the crystal (mounted on a glass plunger) was thoroughly rinsed with the desired solvent and immediately transferred to the infrared cell containing the same solvent with supporting electrolyte and saturated with CO. The spectral thin layer was then formed, as usual, by pushing the electrode up to the CaF_2 window.

Acetonitrile, THF, dichloromethane and methanol were purified and dried prior to use by distillation from the appropriate desiccant (calcium hydride, sodium metal, and P_2O_5, respectively) under dry N_2. Dimethylformamide (Burdick and Jackson) was used as received. The tetrabutylammonium perchlorate (TBAP), tetraethylammonium perchlorate (TEAP), and sodium perchlorate used as supporting electrolytes were recrystallized from methanol, water and ethanol, and water, respectively, and dried under vacuum at 110°C.

Electrode potentials were measured versus the ferrocenium-ferrocene (Fc^+/Fc) couple in the same solvent-supporting electrolyte; this involved the use of an equimolar Fc^+/Fc mixture in contact with a platinum wire in a separate reference compartment. The electrode potentials *quoted* here in each solvent, however, are versus an *aqueous* saturated calomel electrode with a solvent liquid junction formed in the presence of 0.1 M TEAP. While the absolute values of these electrode potentials, E_{SCE}, are still obviously dependent on the choice of reference electrode, *variations* in E_{SCE} even in different solvents should reflect alterations in the desired metal-solution potential drop, ϕ_s^M, since the solvent liquid junction potential is likely to be small ($\lesssim$ 0.1 V) under these conditions (vide infra).[8,17] All measurements were performed at room temperature, 23±1°C.

RESULTS AND DISCUSSION

The experimental strategy pursued here, as in ref. 8, entails obtaining ν_{CO} spectra for saturated CO coverages over wide ranges of electrode potential,

typically between ca -2.0 to 1.0 V vs SCE, by means of potential-difference infrared (PDIR) tactics. As usual,[12,13] these involved subtracting sets of interferometer scans acquired at suitably disparate "sample" and "reference" electrode potentials (E_S and E_R, respectively) so to remove the spectral interference from the thin-layer solvent. Given that potential-dependent sequences of spectra are desired, the procedure most commonly followed involves acquiring sets of interferometer scans during a suitably slow (2 mV s^{-1}) positive-going potential sweep. For solvents containing traces of water, electrooxidative removal of adsorbed CO occurs at high potentials (usually $\gtrsim$ 0.8 V vs SCE), allowing absolute ν_{co} spectra to be obtained by employing a reference spectrum measured at a suitably positive E_R.[8] In rigorously anhydrous solvents, such electrooxidation does not occur, so that bipolar ν_{co} spectra are obtained, featuring band components at both E_R and E_S. This complication, however, does not impair spectral interpretation for suitably disparate E_R and E_S values since the ν_{co} frequencies generally increase towards higher potentials. Indeed, the use of such anhydrous media enables ν_{co} spectra to be obtained for saturated CO coverages even at large positive (ca 1 V) electrode potentials.[8] The infrared results for the various metal surfaces examined here are now described in turn, together with relevant interpretation.

Platinum (110) and (111)

As already mentioned, Pt(110) is of particular interest in the present context since CO is found to bind almost exclusively in a single (terminal) coordination geometry over wide ranges of electrode potential in aqueous media.[3c,5] This property is a cherished one here; ν_{co} frequencies are known to be sensitive to both the overall CO coverage and adlayer structure, so that potential-induced changes in either or both of these factors can have a substantial impact on the observed ν_{co}-E dependencies. [An example of the latter

case is Pt(111), for which an apparently subtle CO adlayer structural transition at ca 0 V vs SCE yields a marked (ca 30%) change in the terminal ν_{co}–E slope.[8]]

A selected sequence of potential-dependent spectra on Pt(110), obtained during a 2 mV s^{-1} potential sweep from -1.6 V vs SCE in CO-saturated dichloromethane containing 0.1 M tetrabutylammonium perchlorate (TBAP), is shown in Fig. 1. Absolute ν_{co} spectra are obtained in this case, since sufficient trace water was present to electrooxidatively remove CO at the E_R value chosen, 1.4 V vs SCE. Only a single ν_{co} band is seen, in the frequency region 2050–2100 cm^{-1} characteristic of terminal ν_{co} binding, throughout the observed potential range.

The plot of the terminal ν_{co} frequency, ν_{co}^t, versus the electrode potential, E, is shown for this system in Fig. 2 (upright triangles). The ν_{co}^t–E trace is seen to be virtually linear, deviations only occurring close to the positive potential limit, at ca 1.0 V vs SCE. Comparable potential-dependent spectra for CO adlayers on Pt(110) were obtained in the other three CO-saturated solvents examined here, containing 0.1 M TBAP. The resulting ν_{co}^t–E data in acetonitrile (circles), methanol (inverted triangles), and THF (squares) are also plotted in Fig. 2. While the ν_{co}^t values in the various solvents at a given electrode potential are seen to differ by up to 5–6 cm^{-1}, the ν_{co}^t–E slopes are virtually solvent independent. (These slopes are also essentially independent of ionic strength, from 0.02 to 2 M.[11]) Closely similar ν_{co}^t–E behavior was observed for saturated CO adlayers on Pt(111), although complicated by a potential-induced adlayer structural transition.[8] The small solvent dependence of ν_{co}^t at fixed E_{SCE} could well be due chiefly to differences in the solvent liquid junction potential, although alterations in the metal-solution potential, ϕ_s^M, due to differing dipole orientation of the solvent juxtaposed with the CO adlayer may partly be responsible.

The quantitative evaluation of the CO coverage, θ_{co}, by the spectrophoto-

metric and faradaic assay of electrochemical CO_2 production, utilized in aqueous media,[12,13,18] is largely precluded here. Nevertheless, saturation coverages close to (within ca 10–20%) that for the Pt(110)/CO–aqueous interface, $\theta_{co} \approx 1.0$,[3c,18] are inferred from the similar integrated absorbances for the terminal band, A_I^t (Table I). In a given solvent, A_I^t, is seen to increase slightly (10%) with increasing potential over the normally accessible range −2.0 to 1.0 V; this likely results chiefly from field-induced effects on the oscillator strength[19] rather than to variations in θ_{co}.

As in our earlier studies,[8,11] it is instructive to scrutinize the effects upon the ν_{co}^t–E behavior in a given solvent of varying the size of the tetraalkylammonium cation. While such experiments are limited by electrolyte solubility constraints, the effect of substituting 0.1 M tetraethylammonium perchlorate (TEAP) for TBAP was examined here. Only a single terminal ν_{co} feature was again observed throughout the accessible potential range. As before, however,[8,11] a significant cation effect upon the ν_{co}^t–E behavior was observed here in acetonitrile and methanol. Figure 3 compares the ν_{co}^t–E dependence obtained for saturated CO on Pt(110) in acetonitrile containing 0.1 M TBAP (open circles) and 0.1 M TEAP (open squares). The ν_{co}^t–E slopes are seen to be significantly different, $d\nu_{co}^t/dE$ being ca 20% larger in TEAP, with the plots intersecting at ca 0.8 V vs SCE. Comparable cation-dependent behavior was also obtained in methanol, and as reported separately for polycrystalline platinum in acetonitrile, methanol, and THF.[11]

These cation dependencies can be understood straightforwardly in terms of electrostatic double-layer effects, and as such yield useful information on the potential-dependent Pt(110) surface charge,[8,11,20] as will now be outlined briefly. The population of excess ionic charge, located at (or close to) the so-called outer Helmholtz plane (oHp), will mirror the excess electronic charge

density, σ_m, located at the metal surface. The potential drop across the CO adlayer, ϕ^M_{co}, will be determined in part by the "free-charge" contribution[2] which is in turn affected by the spatial position of the oHp. The electrode potential where $\sigma_m = 0$ is termed the "potential of zero charge" E_{pzc}; at this point the free-charge contribution to the surface potential vanishes.[2] The electronic charge σ_m is negative when $E < E_{pzc}$ (as will be encountered here), so that the excess ionic charge is then cationic. (This picture ignores specific ionic adsorption, which should, however, be negligible in the presence of saturated CO adlayers.) Substituting TBA^+ by the smaller cation TEA^+ will shift the oHp closer to the metal surface, increasing $-\phi^M_{co}$ at a given electrode potential (or σ_m) and thereby diminishing ν^t_{co}. The magnitude of $-\phi^M_{co}$ will increase as E is lowered further below E_{pzc}; conversely, ϕ^M_{co} will vanish (in the absence of specific ionic adsorption) when $E = E_{pzc}$. (Such potential-distance profiles will be considered further below.)

Consequently, then, the intersection point of the ν^t_{co}-E plots obtained in TEAP and TBAP electrolytes, 0.8 V, should provide an approximate estimate of E_{pzc} for the Pt(110)/CO(sat) system. As noted earlier,[8,11] it is of interest to relate such E_{pzc} values to the surface potentials, ϕ^M_v (vs vacuum), for the corresponding metal-uhv interfaces as deduced from work-function measurements, since the latter system is also uncharged (i.e., $\sigma_m = 0$) in the absence of ionizable adsorbates. Given that the former values are actually potential *differences with respect to a reference electrode*, the required link can be established if the so-called "absolute" potential of the reference electrode, $E_k(ref)$, is known.[21] Thus the metal-solution potential difference, ϕ^M_s, of the electrochemical interface can be related to the measured electrode potential by[2,20,21]

$$\phi^M_s = E + E_k(ref) - \chi_s \qquad (1)$$

where χ_s is the surface potential of the solution–vacuum interface.[21] (This last quantity is commonly expected to be small, $|\chi_s| \lesssim 0.1$–0.2 V.) Given that E_k(ref) ≈ 4.6 (± 0.2) V for the normal hydrogen electrode (NHE)[2], so that E_k(ref) ≈ 4.85 (± 0.2) V for the SCE, the E_{pzc} value determined here for the Pt(110)/CO electrochemical interface, 0.8 V vs SCE, yields from Eq(1) a ϕ_s^M estimate of ca 5.6 V. This estimate is close to the ϕ_v^M value for the Pt(110)/CO(sat)–uhv interface, 5.5 V, deduced from work-function measurements.[3c,22]

A similar comparison for the Pt(111)/CO(sat) system also yielded concordant results.[8] Thus E_{pzc} determined as above for the Pt(111)/CO(sat)–acetonitrile interface, ca 1.0 V vs SCE, yields $\phi_s^M \approx 5.8$ V, to be set alongside the ϕ_v^M value for the Pt(111)/CO(sat)–uhv interface of about 5.9 V.[8,22] Note that the significantly lower ϕ_v^M value for the Pt(110)/CO– versus the Pt(111)CO–uhv interface, as is commonly observed for (110) versus (111) surfaces, is mirrored by a comparably less positive E_{pzc} value for the former electrochemical interface. These comparisons suggest further that the effect of the solvent upon E_{pzc} for the present systems is weak and nonspecific.

Nevertheless, a significant disparity between the uncharged Pt(110)/CO(sat) surface in electrochemical and uhv environments is to be found in the ν_{co} frequencies. Thus the infrared ν_{co}^t values for the latter system ($\theta_{co} = 1.0$) have been reported to be 2115 cm^{-1}[24] or 2130 cm^{-1},[25] while significantly lower values, 2088–2090 cm^{-1}, are seen at E_{pzc} for the present electrochemical systems (Figs. 2,3). A similarly lower ν_{co}^t value for the uncharged electrochemical system has also been deduced by extrapolating ν_{co}^t–E data obtained at the Pt(110)/CO–aqueous interface.[2] The reasons for these disparities are unclear at present, but may be connected with differences in the CO adlayer structure in the electrochemical and uhv systems, perhaps arising from Pt(110) surface reconstruction.[3c]

It is of interest to examine ν_{co}–E behavior in alkali metal as well as

tetraalkylammonium electrolytes. This arises both from the common use of the former electrolytes for related studies in aqueous media,[5] and from the potential-induced alterations in the CO binding site that are observed in nonaqueous solvents containing alkali cations.[10,11] Figure 4 shows a potential-dependent series of infrared spectra for Pt(110) in CO-saturated acetonitrile containing 0.1 M $NaClO_4$ from -1.6 V to 0.9 V vs SCE. A marked, yet reversible, potential-induced spectral change is observed. For potentials below ca -0.8 V, the usual terminal ν_{co} band declines in intensity, being replaced entirely by a weaker band at lower frequencies, 1750-1800 cm^{-1}, by -1.2 V.

Similar potential-induced spectral changes have been observed on polycrystalline platinum, and ascribed to the formation of bridging CO at negative potentials, driven by Lewis acid-base interactions between the alkali cations and the CO adlayer.[11] Figure 5 shows a set of potential-dependent infrared spectra obtained for Pt(111) in CO-saturated acetonitrile containing 0.1 M $NaClO_4$, obtained under similar conditions as in Fig. 4. While the major spectral feature on Pt(111) at higher potentials is a terminal band, unlike Pt(110) a weaker feature is also observed at ca 1840-1860 cm^{-1}, indicative of the additional presence of twofold bridging CO.[5,8] A comparable potential-induced CO site conversion is, nevertheless, seen on Pt(111) as for Pt(110). A pair of differences, however, are that the site conversion takes place at significantly (0.5 V) higher electrode potentials on Pt(111) than Pt(110), and broader- and lower-frequency ν_{co} bands are seen on the former surface (compare Fig. 4 and 5).

The acquisition of ν^t_{co}-E data for Pt(110)/CO(sat) in acetonitrile for such water-soluble double-layer cations also invites comparison with corresponding data obtained in aqueous solutions. Included for this purpose in Fig. 3 are ν^t_{co}-E plots obtained for Pt(110)/CO(sat) in acetonitrile and water (open, filled symbols, respectively) containing 0.1 M TEAP or 0.1 M $NaClO_4$ (squares, upright

triangles, respectively). The potential regions are chosen so that only terminal CO coordination is present; the low-potential limit for the aqueous-based data is limited further by the onset of cathodic hydrogen evolution. Inspection of these data shows that essentially coincident ν_{co}-E traces are obtained in acetonitrile and water containing 0.1 M TEAP. Similarly solvent-independent ν^t_{co}-E behavior is also observed under these conditions on Pt(111).[8]

Somewhat different findings, however, are obtained in 0.1 M $NaClO_4$: while nearly coincident ν^t_{co}-E traces are observed in acetonitrile containing 0.1 M TEAP or $NaClO_4$, in water the latter electrolyte yields significantly higher ν^t_{co}-E slopes that tend to increase towards lower potentials (Fig. 3). Similarly nonlinear ν^t_{co}-E plots are also obtained in aqueous media containing other alkali electrolytes. Of particular earlier interest to us was Pt(110) in 0.1 M NaBr + 0.1 M $HClO_4$, which enables the ν^t_{co}-E dependence to be examined up to higher potentials than is usually the case in aqueous media.[3c,10] These data are included as filled inverted triangles in Fig. 3. The ν^t_{co}-E trace is seen to be coincident with that for 0.1 M $NaClO_4$, yet also merges with that obtained in 0.1 M TEAP in acetonitrile at higher potentials. Discussion of these cation effects will be taken up below, after consideration of related results for Rh(111).

Table I summarizes integrated absorbances, (A^t_i), bandwidths ($\Delta\nu^t_{\frac{1}{2}}$), and ν^t_{co}-E slopes obtained for Pt(110)/CO(sat) in the various media considered here, all referring to the representative potential, -0.2 V vs SCE.

Rhodium (111)

The data presented above for Pt(110), together with that described earlier for Pt(111),[8] show that the solvent exerts little specific influence upon the potential-dependent infrared spectral properties of saturated CO adlayers. Somewhat different results, however, were obtained on Rh(111). Figure 6 shows a potential-dependent spectral sequence obtained on Rh(111) in CO-saturated

aqueous 0.1 M TEAP. The spectra are similar to those obtained earlier in CO-saturated aqueous 0.1 M $NaClO_4$.[9] At the highest potentials (positive of ca 0 V vs SCE), an intense band at 2035-2045 cm^{-1} along with a weaker feature at 1820-1825 cm^{-1} are obtained, attributable to terminal and twofold bridging CO, respectively. At lower potentials (negative of -0.2 V), the intensity of these spectral features diminish sharply, giving way to a new "higher-frequency bridging" feature at 1885-1900 cm^{-1}. This potential-induced structural transition is reversible. Such infrared spectra combined with corresponding in-situ atomic-resolution scanning tunneling microscopy (STM) have recently enabled us to deduce the real-space CO adlayer structures for this system in some detail.[9] Briefly, a (2x2)-3CO structure (θ_{co} = 0.75) is obtained at high potentials, featuring two near-atop and one twofold bridging CO in the unit cell. At low potentials, a (3 x $\sqrt{3}$ rect)-4CO structure (θ_{co} = 0.67) is formed which consists of only one atop CO per unit cell, the remaining 3 CO's occupying twofold bridging sites of which two are asymmetric in character. The CO adlayer structural transition therefore involves a terminal/bridging site conversion.

The use of dilute (down to 5 mM) aqueous $HClO_4$ in place of TEAP or $NaClO_4$ electrolytes yielded similar potential-dependent spectra, although the terminal/bridging structural transition occurs at significantly lower potentials, at ca -0.3 V vs SCE. A markedly greater sensitivity of the potential-dependent spectra to the supporting-electrolyte cation, however, was obtained for Rh(111) in CO-saturated acetonitrile. With 0.1 M $NaClO_4$, the terminal/bridging CO site conversion occurs at a higher potential, 0.4 V vs SCE. At more negative potentials, below ca -1.0 V, the "high-frequency bridging" feature at 1850-1890 cm^{-1} gives way to a lower-frequency bridge band, at 1780-1825 cm^{-1}. In CO-saturated acetonitrile containing 0.1 M TEAP, however, no clearcut potential-induced site conversion was observed, spectra characteristic of the usual "high-

potential" adlayer structure, i.e., featuring predominantly terminal CO coordination, being observed throughout the readily accessible potential range, from -2.0 to 1.0 V vs SCE. Similar behavior was also observed using 0.1 M TBAP as supporting electrolyte. Comparable electrolyte-dependent results were also obtained in methanol, although unlike those in acetonitrile some partial terminal/bridging site conversion was discernable in 0.1 M TEAP at potentials below ca 0 V vs SCE.

These results for Rh(111)/CO(sat) are collated in Figs. 7 and 8 in the form of plots of the terminal and bridging ν_{co} frequencies, ν_{co}^{t} and ν_{co}^{b}, respectively, versus the electrode potential, for conditions where the "high-potential" adlayer structure predominates (so that the site occupancies are effectively invariant with potential). The open circles, squares, and upright triangles refer to acetonitrile containing 0.1 M TBAP, TEAP, and $NaClO_4$, respectively; the filled squares, upright triangles, and inverted triangles denote aqueous 0.1 M TEAP, 0.1 M $NaClO_4$, and 5 mM $HClO_4$, respectively.

Similarly to the platinum surfaces, the ν_{co}^{t}-E and ν_{co}^{b}-E plots for Rh(111)/CO(sat) in acetonitrile containing 0.1 M TBAP and TEAP are seen to exhibit straight lines with dissimilar slopes, intersecting at ca 0.9-1.0 V vs SCE (Figs. 7,8). This E_{pzc} estimate, yielding $\phi_s^M \approx 5.8$ V from Eq(1), is approximately consistent with the ϕ_v^M value for the Rh(111)/CO(sat)-uhv interface, ca 5.9 V.[26] The terminal and bridging ν_{co} frequencies at this potential, ca 2060 and 1850 cm^{-1}, are close to those measured, 2065 and 1855 cm^{-1},[30] for an apparently similar (2x2)-3CO structure on Rh(111) in uhv.[9,29] As on Pt(110), the ν_{co}^{t}-E segment obtained for acetonitrile/$NaClO_4$ is virtually coincident with that for TEAP, although the onset of terminal/bridge site conversion limits severely the accessible potential range in the former electrolyte (Fig. 7). The presence of more specific coupled solvent/cation effects, however, can be discerned by

comparing the ν^t_{co}–E and especially the ν^b_{co}–E plots in acetonitrile/TEAP and water/TEAP (and water/$NaClO_4$) in Figs. 7 and 8. The higher slopes and lower ν_{co} frequencies obtained in the latter solvent are clearly evident, to a markedly greater extent than for Pt(110) (Fig. 3). By and large, these specific effects are attenuated for electrode potentials approaching E_{pzc}, as can be seen by extrapolating the aqueous-based ν^t_{co}–E and ν^b_{co}–E plots to E_{pzc}, ca 0.9–1.0 V.

In a similar manner to Pt(110) (Table I), Table II summarizes integrated absorbances, bandwidths, and ν_{co} frequency–potential slopes for the terminal and also bridging CO features obtained for Rh(111)/CO(sat) in selected solvent media; these data refer to an electrode potential, 0.1 V vs SCE, where the "high-potential" adlayer structure is present in each case.

General Discussion: Band Frequency–Potential Dependencies

When combined with the results of our related study on Pt(111)[8] together with our corresponding data for single-crystal Pt- and Rh-aqueous interfaces,[2,5] the present findings provide a uniquely detailed assessment of the manner in which the addition of excess negative charge to the metal surface, corresponding to electrode potentials progressively below E_{pzc}, can affect the CO adsorbate bonding properties as manifested in the infrared spectra. Of particular fundamental interest is the opportunity afforded, especially on Pt(110), to examine the ν^t_{co}–E dependencies at fixed adsorption site occupancy over wide ranges (up to 3 V) of electrode potential. This general phenomenon, by which adsorbate vibrational frequencies shift with potential, has captured the attention of electrochemists since the early days of in-situ vibrational spectroscopies.[31] The occurrence of a first-order Stark effect (due to changes in the local electrostatic field) and/or the presence of potential-dependent adsorbate-metal charge sharing have been forwarded as alternative explanations for the observed frequency–potential dependencies, most notably for adsorbed CO

(refs. 32-36 are representative). Especially since we have recently discussed our extensive frequency-potential data for monocrystalline metal-aqueous interfaces with respect to these predictions,[2,5,10] it is pertinent to assess how the more diverse data now available may contribute to our understanding of this phenomena (often loosely termed the "Stark-tuning" effect).

By and large, the trends in the ν_{co}-E dependencies observed for a given surface in nonaqueous and aqueous media are readily compatible. The experimental conditions, both with regard to the ranges of electrode potentials and the nature of the double-layer cations, tend to differ in these two cases due to the limits imposed by solvent decomposition and electrolyte solubility. Two behavioral differences nevertheless emerge that are worth highlighting. First, the ν^t_{co}-E (and ν^b_{co}-E) slopes tend to be smaller in nonaqueous solvents (Tables I, II). This difference is partly attributable to the tendency to use larger cations in nonaqueous media; thus Pt(110)/CO yields near-identical ν^t_{co}-E behavior in acetonitrile and water containing 0.1 M TEAP (Fig. 3). However, $NaClO_4$ electrolyte yields noticeably larger ν^t_{co}-E slopes on both Pt(110) and Rh(111) in water versus acetonitrile (Figs. 3, 7). Second, the ν^t_{co}-E (and ν^b_{co}-E) dependencies are essentially linear over 2-3 V in the nonaqueous media examined here, provided that potential-induced changes in adlayer structure (or coverage) are absent. This finding differs from that in aqueous media, where we have uncovered significantly nonlinear ν^t_{co}-E behavior, especially for Pt(110)/CO, the slopes increasing towards lower potentials.[10]

Inspecting Figs. 3 and 7, these two differences are seen to be manifested in ν^t_{co} values in aqueous media, especially with $NaClO_4$ electrolyte, that tend to fall increasingly below the linear ν^t_{co}-E traces observed in acetonitrile (and other nonaqueous solvents) as the potential is lowered. This observation suggests that the differing behavior in aqueous media, rather than being due

entirely to the intrinsic CO adlayer properties (as might be presumed in the absence of the nonaqueous data[2]), actually arise partly from the vagaries of the aqueous double-layer environment.

In order to rationalize these coupled solvent/cation effects, it is useful to consider a conventional electrochemical double-layer model in which the metal-solution potential drop, ϕ_s^M, is contained chiefly between the metal surface and the oHp formed by the electrolyte cations. The distance over which the potential drop occurs is therefore determined by the sum of the CO adlayer thickness and the effective cation radius, $(d_{co} + r_c)$. Irrespective of the physical origin(s) of the ν_{co}–E dependencies, the band frequency should respond only to the portion of the potential drop which lies across the CO adlayer itself, ϕ_{co}^M. In the simplest case where the potential changes linearly with distance, d, between the metal and the oHp, i.e., assuming that the inner-layer field is independent of d, ϕ_{co}^M is related to ϕ_s^M by

$$\phi_{co}^M = \phi_s^M \, [d_{co}/(d_{co} + r_c)] \tag{2}$$

Given that $dE = d\phi_s^M$, the measured ν_{co}–E dependence, $d\nu_{co}/dE$ (often termed the "Stark-tuning rate"), can be related to the desired quantity $d\nu_{co}/d\phi_{co}^M$ by[11]

$$(d\nu_{co}/dE)^{-1} = [(d_{co} + r_c)/d_{co}](d\nu_{co}/d\phi_{co}^M)^{-1} \tag{3}$$

Strictly speaking, ϕ_s^M (and hence $d\phi_s^M$ and dE) also differs from ϕ_{co}^M by the potential drop across the diffuse layer, ϕ_{diff}. However, the contribution of this factor as gauged by the quantity $(d\phi_{diff}/dE)$ is probably small or negligible under the present circumstances. Estimates of $(d\phi_{diff}/dE)$ obtained from Gouy-Chapman theory combined with the values of E_{pzc} and the typical double-layer capacitance, $6\mu F\ cm^{-2}$ [measured for Pt(111)/CO in acetonitrile[37]], vary from roughly 0.07 for 0.02 M electrolyte to 0.035 at 2 M ionic strength over the potential range −1.5

to 0.5 V vs SCE, of primary interest here. These small values of ($d\phi_{diff}/dE$) are in harmony with the observed minor (or negligible) effects of electrolyte ionic strength upon both ν_{co}^{t} and ($d\nu_{co}^{t}/dE$) on Pt(110)[5] and polycrystalline Pt.[11]

As noted in ref. 11, Eq(3) can account semiquantitatively for the observed variations in $d\nu_{co}^{t}/dE$ arising from altering the size of the tetraalkylammonium cation. A similar finding applies here [and to the Pt(111) data in ref. 8], although only a pair of such cations were examined. Thus assuming that $d_{co} \approx 3.2$Å,[8] and that $r_c = 4.0$ and 5.0Å for TEA^+ and TBA^+, respectively (from their crystallographic radii[8,38]), a ratio of $d\nu_{co}/dE$ values in TEAP and TBAP electrolytes is predicted from Eq(3) to be 1.15, to be compared with the experimental $d\nu_{co}^{t}/dE$ and $d\nu_{co}^{b}/dE$ values that range from 1.1 to 1.4 (Tables I, II, and also from Table I of ref. 8). This tendency to underestimate the observed cation effect may arise from several factors, such as uncertainties in the inner-layer geometry and the inevitable limitations of the *simple constant-field* (and average-potential) model embodied in Eq(3).

These considerations suggest that the larger, and potential-dependent, $d\nu_{co}/dE$ values obtained in aqueous media, especially with alkali metal electrolytes, arise from differences in the spatial and dielectric properties of the double-layer cation in aqueous compared with nonaqueous environments. Examination of the ν_{co}^{t}–E data for Pt(110) (Fig. 3) shows that the plot in aqueous 0.1 M $NaClO_4$ swings further below the corresponding trace in acetonitrile (filled and open upright triangles, respectively) as the potential is lowered. A plausible explanation is that the oHp formed by such alkali cations is situated closer to the CO adlayer in the aqueous media, and especially so towards lower potentials. This infers that the effective Na^+ r_c value in Eq(3) (i.e., the solvated radius of the oHp cation) is smaller in water than in acetonitrile, at least towards more negative electrode charges, i.e., negative ($E-E_{pzc}$) values.

An alternative, and perhaps more attractive, explanation is that the superior electrostatic screening properties of water diminish the electrostatic fields outside the CO adlayer, so that a greater fraction of the ϕ_s^M falls within this layer, yielding larger $d\nu_{co}/dE$ values than predicted from Eq(3). This latter explanation is compatible with the observed insensitivity of the ν_{co}^t–E behavior at the Pt(110)/CO–aqueous interface to the nature of the hydrated electrolyte cation (Na^+, Ca^{2+}, La^{3+}, etc.).[3c] Similar arguments can be applied to the Rh(111) data in Fig. 7. While necessarily speculative, these points illustrate that consideration of the more diverse ν_{co}–E data set afforded by including nonaqueous media can yield fresh insight into the behavior of the more familiar aqueous-based systems.

Given the simple form of Eq(3), it is tempting to provide estimates of the "true Stark-tuning rate" $d\nu_{co}/d\phi_{co}^M$, i.e., the sensitivity of the band frequency to the potential drop across *only* the CO adlayer. In view of the relative values of d_{co} and r_c noted above, given that $d\nu_{co}^t/dE$ is typically about 20(±4) cm^{-1} V^{-1} in the tetraalkylammonium electrolytes for Pt(110) and Rh(111) (Tables I, II), one can deduce from Eq(3) that the required estimates of $d\nu_{co}^t/d\phi_{co}^M$ will be roughly 2.2–2.5 times larger, say 50 (±10) cm^{-1} V^{-1}. Somewhat (ca 20–30%) higher $d\nu_{co}^b/d\phi_{co}^M$ values are inferred on this basis for Rh(111) (Table II), in harmony with earlier findings.[2,5]

Comparison with Band Frequency-Electrostatic Field Dependencies in UHV

It is also of interest to compare anew such $d\nu_{co}/d\phi_{co}^M$ estimates with the related quantities obtained in metal–uhv environments (cf ref. 2).[32] Specifically, Lambert and coworkers[39] have evaluated "Stark-tuning rates" for Pt(111)/CO expressed in terms of the electric field $\mathcal{E}$ rather than the electrode potential across the CO adlayer. The former quantity is set equal to the modulating field established between the substrate surface and a nearby counter electrode in

uhv.[32] Transposition of the $d\nu_{co}/d\mathcal{E}$ and $d\nu_{co}/d\phi^{M}_{co}$ values can be made using

$$d\nu_{co}/d\mathcal{E} = d_{co}(d\nu_{co}/d\phi^{M}_{co}) \qquad (4)$$

From the $d\nu_{co}/d\mathcal{E}$ data for Pt(111)/CO(sat) given in ref. 39, $d\nu^{t}_{co}/d\phi^{M}_{co}$ and $d\nu^{b}_{co}/d\phi^{M}_{co}$ values of ca 10 and 15 cm^{-1} V^{-1}, respectively, are extracted from Eq(4) by assuming that d_{co} = 3.5Å (as in ref. 32). These values are markedly smaller than the corresponding $d\nu^{t}_{co}/d\phi^{M}_{co}$ and $d\nu^{b}_{co}/d\phi^{M}_{co}$ estimates extracted from the Pt(111)/CO(sat)–nonaqueous data in ref. 8. Thus at high potentials (E > 0 V vs SCE) in acetonitrile/TBAP, for example, $d\nu^{t}_{co}/dE$ = 20 cm^{-1} V^{-1} and $d\nu^{b}_{co}/dE$ = 23.5 cm^{-1} V^{-1}; based on Eq(3) the corresponding $d\nu_{co}/d\phi^{M}_{co}$ estimates are about 2.5 fold larger. Even if Eq(3) is considered quantitatively unreliable, the measured $d\nu^{t}_{co}/dE$ values provide at least *lower limits* for $d\nu^{t}_{co}/d\phi^{M}_{co}$; these are still ca twofold larger than the corresponding uhv values.

What is the origin of the unexpectedly smaller Stark tuning slopes for Pt(111)/CO in the uhv compared with the electrochemical environments? It is possible that the actual electrostatic field across the CO adlayer is less than the measured average field between the electrodes in uhv. Such disparities are more likely for the metal–uhv system since the fraction of the potential drop located across the CO adlayer ϕ^{M}_{co} is only a tiny fraction of the overall potential difference applied between the two electrodes. In the electrochemical case, a substantial fraction ($\gtrsim$ 50%) of the metal–solution potential drop ϕ^{M}_{s} falls across the CO adlayer, since ϕ^{M}_{s} is confined necessarily to molecular-level distances from the metal substrate. As a consequence, the extraction of the required $d\nu_{co}/d\phi^{M}_{co}$ estimates from the observed $d\nu_{co}/dE$ values is semiquantitatively reliable. In addition, the field strength established in such uhv-based experiments, ca 3 x 10^{4} V cm^{-1}, is much (ca 10^{3} fold) smaller than that established in the electrochemical systems. The former measurements therefore

refer to small displacements in ϕ^{M}_{co} away from the value corresponding to the uncharged Pt(111)/CO–uhv interface, which as noted above is analogous to E_{pzc}. Indeed, markedly diminished $d\nu^{t}_{co}/dE$ slopes are observed for Pt(111)/CO–THF and other nonaqueous systems at high electrode potentials, in the vicinity of and above E_{pzc}, 1.0 V vs SCE (see Fig. 2 of ref. 8). Such measurements are difficult to undertake reliably since even small traces of water can electrooxidize adsorbed CO under these conditions (and oxidatively disorder the metal surface!); nevertheless, the effect appears to be reproducible. It is feasible, therefore, that the smaller "Stark-tuning rates" observed for Pt(111) in uhv reflect the occurrence of nonlinear field effects, rather than to a more intrinsic behavioral difference between the electrochemical and uhv environments.

It is also appropriate to note in this context an interesting potential dependence of the dynamical dipole–dipole coupling for the Pt(111)/CO(sat)–acetonitrile (0.1 M TBAP) system, observed from $^{12}CO/^{13}CO$ isotopic dilution experiments.[40] These measurements show that the frequency upshifts of the terminal ν_{co} band due to dipole coupling, $\Delta\nu^{t}_{D}$, diminish markedly, from about 35–40 cm^{-1} at ca 0 V vs SCE to 15 cm^{-1} at ca −2 V. A substantial fraction, about 0.5–0.7, of the ν^{t}_{co}–E slope observed under these conditions, 13 cm^{-1} V^{-1},[8] can therefore be ascribed to potential-dependent dipole coupling, even though $\Delta\nu_{D}$ remains roughly constant for potentials between 0 and 1 V vs SCE.[40] This finding indicates that the factors that influence Stark-tuning slopes in electrochemical systems can be unexpected as well as potential dependent.

Potential-Dependent Adsorption Geometries

It remains to consider the ramifications of the coupled solvent/cation effects on the potential-dependent CO site conversions observed for the present systems. The terminal/bridging coordination shifts induced by Na^{+}, noted here for Pt(110), Pt(111), and Rh(111) in acetonitrile, are similar to those discussed

elsewhere for polycrystalline Pt.[11] Briefly, the alkali cation appears to act as a Lewis acid towards the adsorbed carbonyl oxygen (cf ref. 41). This interaction should be preferred for bridging CO as a consequence of the greater electron density on the oxygen afforded by $d\pi \rightarrow 2\pi^*$ back bonding.[11] The presence of alkali cations at the oHp should therefore aid the terminal-bridging site conversion brought about by enhanced back bonding as the negative electrode charge is increased,[2] i.e., towards lower electrode potentials.

The propensity for terminal-bridging site conversion, as adjudged by the electrode potential at which the coordination shifts for the saturated CO adlayer occurs, lies in the sequence Pt(110) < Pt(111) < Rh(111). This order is the same as that found for potential-induced site conversion in the apparent absence of specific cation effects, such as in water/TEAP or other aqueous media.[5] More surprising is the observation of specific cation/solvent effects upon the CO site conversion on Rh(111). Thus the complete absence of this coordination shift in acetonitrile/TEAP or TBAP, even down to -2 V vs SCE, contrasts the presence of such site conversion for Rh(111)/CO(sat) in water/TEAP (Fig. 6). Nevertheless, the similar potential-dependent behavior of the latter system to water/$NaClO_4$ would appear to implicate a coupled influence of the solvent and the supporting electrolyte cation. This more "solvent/cation-specific" nature of the Rh(111)/CO system as compared to Pt(110)/CO [or Pt(111)/CO] can, however, be gleaned from the noticeably more deviant ν_{co}-E plots obtained in water and acetonitrile for the former compared to the latter surface (compare Figs. 7, 8, and 3).

While such trends therefore signal a role for the specific solvation factors anticipated for such systems, the present findings by and large support the notion of satisfying simplicity provided by the earlier Pt(111)/CO results.[8] In particular, the ν_{co}-E behavior observed for a given CO adlayer structure on all three surfaces, especially Pt(110) and Pt(111), display a notable insensitiv-

ity to the solvent medium along with a systematic dependence upon the nature of the double-layer cation. The latter effects also assist the comparison of such spectral information for electrochemical systems with vibrational data for the corresponding metal-uhv interfaces in enabling E_{pzc}, and hence ϕ_s^M, for the former surfaces to be assessed.

CONCLUDING REMARKS

Taken together, then, the present results add significantly to the notion, highlighted elsewhere,[2] that the surface potential (and the accompanying electronic charge density) influence the structure and bonding of CO adlayers on ordered electrochemical surfaces in predictable ways that can be linked directly to the behavior of related metal-uhv systems. These findings are satisfying in that they suggest that at least some of the often-marked behavioral dissimilarities between such electrochemical and uhv systems may be rationalized and even predicted based on the known differences in surface potential. While the measurement, let alone the control, of the surface potential and attendant electrostatic fields in metal-uhv systems is relatively uncommon, a greater attention to such effects would appear to be well justified.

It should be stressed that the present findings do not in themselves provide a demarcation between the alternative descriptions of band frequency-electrode potential dependencies based on electrostatic field (first-order Stark) effects and metal-adsorbate charge sharing.[32,34] Nevertheless, some aspects of the present data can be usefully set against specific predictions of these models. For example, the marked nonlinearities in the ν_{co}-E behavior over the present extended ranges of electrode potential (> 1 V) that are predicted by some molecular orbital calculations, yielding large (> 100 cm^{-1} V^{-1}) $d\nu_{co}^t/dE$ values at low potentials,[34,42] are certainly not borne out by the present findings. The earlier nonlinear ν_{co}-E data obtained at monocrystalline metal-aqueous

interfaces, which appeared to yield some support to these theoretical findings,[10] are now surmised to be due primarily to environmental double-layer effects.

While it is clear that the roles of the solvent and ionic charges, ever-present in electrochemical systems, certainly cannot be ignored even when dealing with saturated chemisorbate layers, they tend to modify rather than dominate the observed potential-dependent spectral behavior. In this regard, it would be of particular interest to pursue further experimental connections between the electrochemical and uhv surface behavior, specifically by examining the coupled effects upon the ν_{co} spectra and surface potential of dosing components of the former systems in uhv environments (cf ref. 1). We hope to report on experiments of this type in the near future.

ACKNOWLEDGMENTS

We thank Si-Chung Chang for experimental advice and assistance, and for helpful discussions. This work is supported by the National Science Foundation and the Office of Naval Research.

REFERENCES

1. For example: (a) J.K. Sass, K. Bange, ACS Symp. Ser., 378 (1988), 54, and earlier references quoted therein; (b) F.T. Wayner, T.E. Moylan, ACS Symp. Ser., 378 (1988), 65

2. For an overview, see: S.-C. Chang, M.J. Weaver, J. Phys. Chem., 95 (1991), 5391

3. (a) S.-C. Chang, M.J. Weaver, J. Chem. Phys., 92 (1990), 4582; (b) S.-C. Chang, M.J. Weaver, J. Phys. Chem., 94 (1990), 5095; (c) S.-C. Chang, M.J. Weaver, Surface Science, 230 (1990), 222

4. (a) L.-W.H. Leung, S.-C. Chang, M.J. Weaver, J. Chem. Phys., 90 (1989), 7426; (b) S.-C. Chang, M.J. Weaver, J. Electroanal. Chem., 285 (1990), 263

5. S.-C. Chang, M.J. Weaver, Surface Science, 238 (1990), 142

6. X. Jiang, S.-C. Chang, M.J. Weaver, J. Phys. Chem., 95 (1991), 7453

7. (a) F. Kitamura, M. Takeda, M. Takahashi, M. Ito, Chem. Phys. Lett., 142 (1987), 318; (b) F. Kitamura, M. Takahashi, M. Ito, Surface Science, 223 (1989), 493

8. S.-C. Chang, X. Jiang, J.D. Roth, M.J. Weaver, J. Phys. Chem., 95 (1991), 5378

9. S.-L. Yau, X. Gao, S.-C. Chang, B.C. Schardt, M.J. Weaver, J. Am. Chem. Soc., 113 (1991), 6049

10. J.D. Roth, S.-C. Chang, M.J. Weaver, J. Electroanal. Chem., 288 (1990), 285

11. J.D. Roth, M.J. Weaver, Langmuir, in press

12. S.-C. Chang, M.J. Weaver, J. Chem. Phys., 92 (1990), 4582

13. D.S. Corrigan, M.J. Weaver, J. Electroanal. Chem., 241 (1988), 143

14. D. Zurawski, L. Rice, M. Hourani, A. Wieckowski, J. Electroanal. Chem., 230 (1987), 221

15. L.-W.H. Leung, A. Wieckowski, M.J. Weaver, J. Phys. Chem., 92 (1988), 6985

16. L.-W.H. Leung, S.-C. Chang, M.J. Weaver, J. Chem. Phys., 90 (1989), 7426

17. J.W. Diggle, A.J. Parker, Electrochim. Acta, 18 (1973), 975

18. M.J. Weaver, S.-C. Chang, L.-W.H. Leung, X. Jiang, M. Rubel, M. Szlarczyk, D. Zurawski, A. Wieckowski, J. Electroanal. Chem., in press.

19. D.K. Lambert, J. Chem. Phys., 94 (1991), 6237

20. X. Gao, S.-C. Chang, X. Jiang, A. Hamelin, M.J. Weaver, J. Vac. Sci. Tech. A, in press

21. S. Trasatti, J. Electroanal. Chem., 150 (1983), 1

22. Slightly (0.2 eV) higher work functions for CO-covered low-index platinum surfaces have been obtained by means of photoemission measurements on polycrystalline surfaces with apparent monocrystalline facets.[23]

23. H.H. Rotermund, S. Jakubith, S. Kubala, A. Von Oertzen, G. Ertl, J. Electron. Spect. Related Phenom., 52 (1990), 811

24. S.R. Bare, P. Hofmann, D.A. King, Surface Science, 144 (1984), 347

25. B.E. Hayden, A.W. Robinson, P.M. Tucker, Surface Science, 192 (1987), 163

26. This value is extracted from the known work function for clean Rh(111), 5.2 eV,[27], together with the work-function increase, ca 0.7 eV, upon CO adsorption[28] [to yield a (2x2)-3CO structure[29] similar to that seen in the high-potential electrochemical environment.[9]]

27. Estimated from data cited in ref. 4a

28. E. Bertel, G. Rosina, F.P. Netzer, Surface Science, 172 (1986), L515

29. M.A. Van Hove, R.J. Koestner, J.C. Frost, G.A. Somorjai, Surface Science, 129 (1983), 482

30. L.H. DuBois, G.A. Somorjai, Surface Science, 91 (1980), 514

31. For example: (a) A.B. Anderson, R. Kötz, E. Yeager, Chem. Phys. Lett., 82 (1981), 130; (b) P. Gao, M.J. Weaver, J. Phys. Chem., 90 (1986), 4057

32. D.K. Lambert, J. Chem. Phys., 89 (1988), 3847; and references cited therein

33. S. Holloway, J.K. Norskov, J. Electroanal. Chem., 161 (1984), 193

34. A.B. Anderson, J. Electroanal. Chem., 280 (1990), 37

35. C. Korzeniewski, S. Pons, P.P. Schmidt, M.W. Severson, J. Chem. Phys., 85 (1986), 4153

36. P.S. Bagus, G. Pacchioni, Surface Science, 236 (1990), 233

37. J.D. Roth, G.J. Lewis, L.K. Safford, X. Jiang, L.F. Dahl, M.J. Weaver, J. Am. Chem. Soc., in press

38. From a compilation in: E.R. Nightingale, Jr., J. Phys. Chem., 63 (1959), 1381

39. (a) J.-S. Luo, R.G. Tobin, D.K. Lambert, F.T. Wagner, T.E. Moylan, J. Electron Spectrosc. Relat. Phenom., 54/55 (1990), 469; (b) D.K. Lambert, personal communication

40. J.D. Roth, G.J. Lewis, X. Jiang, L.F. Dahl, M.J. Weaver, J. Phys. Chem., submitted

41. For example: (a) D.F. Shriver, J. Organomet. Chem., 94 (1975), 259; (b) M.Y. Darensbourg, Prog. Inorg. Chem., 33 (1985), 221

42. For example: S.P. Mehandru, A.B. Anderson, J. Phys. Chem., 93 (1989), 2044

TABLE I Representative Infrared Data for Saturated CO Adlayers on Pt(110) in Various Solvent Media at −0.2 V vs SCE

Solvent	Electrolyte[a]	A_i^t[b] cm^{-1}	$\Delta\nu_i^t$[c] cm^{-1}	$d\nu_{co}^t/dE$[d] $cm^{-1}\ V^{-1}$
Acetonitrile	0.1 M TBAP	0.14	11	17.2
	0.1 M TEAP	0.15	12	21.2
	0.1 M $NaClO_4$	0.12	12	21.0
Methanol	0.1 M TBAP	0.17	11	15.0
	0.05 M TEAP[e]	0.18	12	21.2
Dichloromethane	0.1 M TBAP	0.16	11	16.8
THF	0.1 M TBAP	0.12	12	15.0
Water	0.1 M TEAP	0.17	10	19.8
	0.1 M $NaClO_4$	0.16	15	32.6
	0.1 M NaBr + 0.1 M $HClO_4$	0.12	13	31.2

[a] TBAP = tetrabutylammonium perchlorate; TEAP = tetraethylammonium perchlorate

[b] Integrated absorbance of terminal ν_{co} band at −0.2 V

[c] Full width at half maximum absorbance of terminal ν_{co} band at −0.2 V

[d] Slope of ν_{co}^t–E plot at −0.2 V

[e] Saturation electrolyte concentration

TABLE II Representative Infrared Data for Saturated CO Adlayers on Rh(111) in Selected Solvent Media at 0.1 V vs SCE

Solvent	Electrolyte	A_i^t[a] cm^{-1}	$\nu_{\frac{1}{2}}^t$[b] cm^{-1}	$d\nu_{co}^t/dE$[c] $cm^{-1}\ V^{-1}$	A_i^b[d] cm^{-1}	$\Delta\nu_{\frac{1}{2}}^b$[e] cm^{-1}	$d\nu_{co}^b/dE$[f] $cm^{-1}\ V^{-1}$
Acetonitrile	0.1 M TBAP	0.10	12	14.0	0.02	14	18.3
	0.1 M TEAP	0.08	13	18.2	0.04	19	22.0
Methanol	0.05 M TEAP[g]	0.15	15	17.2	0.02	17	22.6
Water	0.1 M TEAP	0.10	12	28.4	0.02	15	30.5
	0.1 M $NaClO_4$	0.08	14	29.6	0.02	18	46.0
	5 mM $HClO_4$	0.09	15	29.2	0.03	20	41.3

[a] Integrated absorbance of terminal ν_{co} band at 0.1 V

[b] Full width at half maximum absorbance of terminal ν_{co} band

[c] Slope of ν_{co}^t–E plot at 0.1 V

[d] Integrated absorbance of twofold bridging ν_{co} band at 0.1 V

[e] Full width at half maximum absorbance of twofold bridging ν_{co} band

[f] Slope of ν_{co}^b–E plot at 0.1 V

[g] Saturation electrolyte concentration

FIGURE CAPTIONS

Fig. 1

Sequence of infrared absorbance spectra in C–O stretching region for CO adlayer on Pt(110) in CO–saturated dichloromethane containing 0.10 M TBAP obtained during positive-going potential sweep at 2 mV s^{-1} from –1.60 V vs SCE. Each spectrum involved acquiring 100 interferometer scans (consuming ca 1 min.), subtracted from which was a similar set of scans acquired after complete CO electrooxidation, at 1.45 V. Potentials indicated alongside each spectrum are average values (vs SCE) during the spectral acquisition.

Fig. 2

Plots of peak frequency of terminal C–O stretch, ν^{t}_{CO}, versus electrode potential for CO adlayer on Pt(110) in CO–saturated solvents containing 0.1 M TBAP as indicated: circles, acetonitrile; inverted triangles, methanol; upright triangles, dichloromethane; squares, THF.

Fig. 3

Plots of peak frequency of terminal C–O stretch, ν^{t}_{CO}, versus electrode potential for CO adlayer on Pt(110) in CO–saturated solvents as indicated: open circles, acetonitrile + 0.10 M TBAP; open squares, acetonitrile + 0.10 M TEAP; open upright triangles, acetonitrile + 0.10 M $NaClO_4$; filled squares, water + 0.10 M TEAP; filled upright triangles, water + 0.10 M $NaClO_4$; filled inverted triangles, water + 0.10 M NaBr + 0.10 M $HClO_4$.

Fig. 4

Sequence of infrared absorbance spectra in C–O stretching region for CO adlayer on Pt(110) in CO–saturated acetonitrile containing 0.10 M $NaClO_4$. Each spectrum involved acquiring 100 interferometer scans subtracted from which was a similar reference set. The top six spectra were obtained during a positive-going potential sweep at 2 mV s^{-1}, and their reference acquired at 1.6 V, after complete CO electrooxidation. The bottom two spectra were obtained during a negative-going potential sweep, their reference being obtained at 0.30 V. Potentials indicated for each spectrum are average values (vs SCE) during the spectral acquisition.

Fig. 5

Sequence of infrared absorbance spectra in C–O stretching region for CO adlayer on Pt(111) in CO–saturated acetonitrile containing 0.15 M $NaClO_4$, obtained as noted in caption to Fig. 1.

Fig. 6

Sequence of infrared absorbance spectra in C–O stretching region for CO adlayer on Rh(111) in CO-saturated aqueous solution containing 0.10 M TEAP obtained during positive-going potential sweep at 1 mV s^{-1} from –0.40 V vs SCE. Each spectrum involved acquiring 100 interferometer scans subtracted from which was a similar set of scans acquired after complete CO electrooxidation, at ca 0.5 V.

Fig. 7

Plots of peak frequency of terminal C–O stretch, ν^{t}_{CO}, versus electrode potential for CO adlayer on Rh(111) in CO-saturated solvents as indicated: circles, acetonitrile + 0.1 M TBAP; open squares, acetonitrile + 0.10 M TEAP; open upright triangles, acetonitrile + 0.1 M $NaClO_4$; filled squares, water + 0.10 M TEAP; filled upright triangles, water + 0.10 M $NaClO_4$; filled inverted triangles, water + 5 mM $HClO_4$.

Fig. 8

Plots of peak frequency of bridging C–O stretch, ν^{b}_{CO}, versus electrode potential for CO adlayer on Rh(111) in CO-saturated solvents as indicated in caption to Fig. 7.

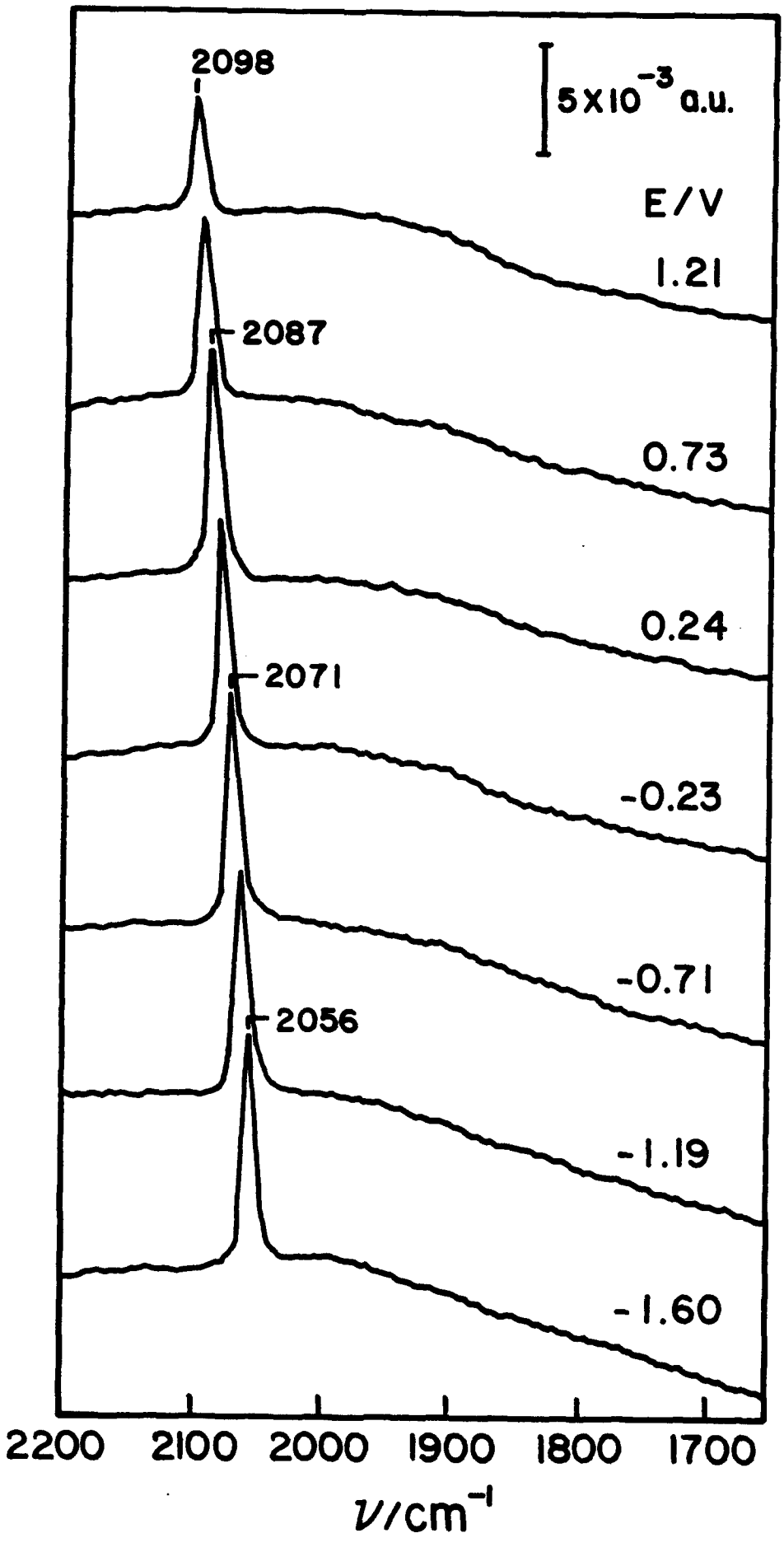
2098
5X10⁻³ a.u.
E/V
1.21
2087
0.73
0.24
2071
-0.23
-0.71
2056
-1.19
-1.60
2200
2100
2000
1900
1800
1700
ν/cm⁻¹

Fig. 1

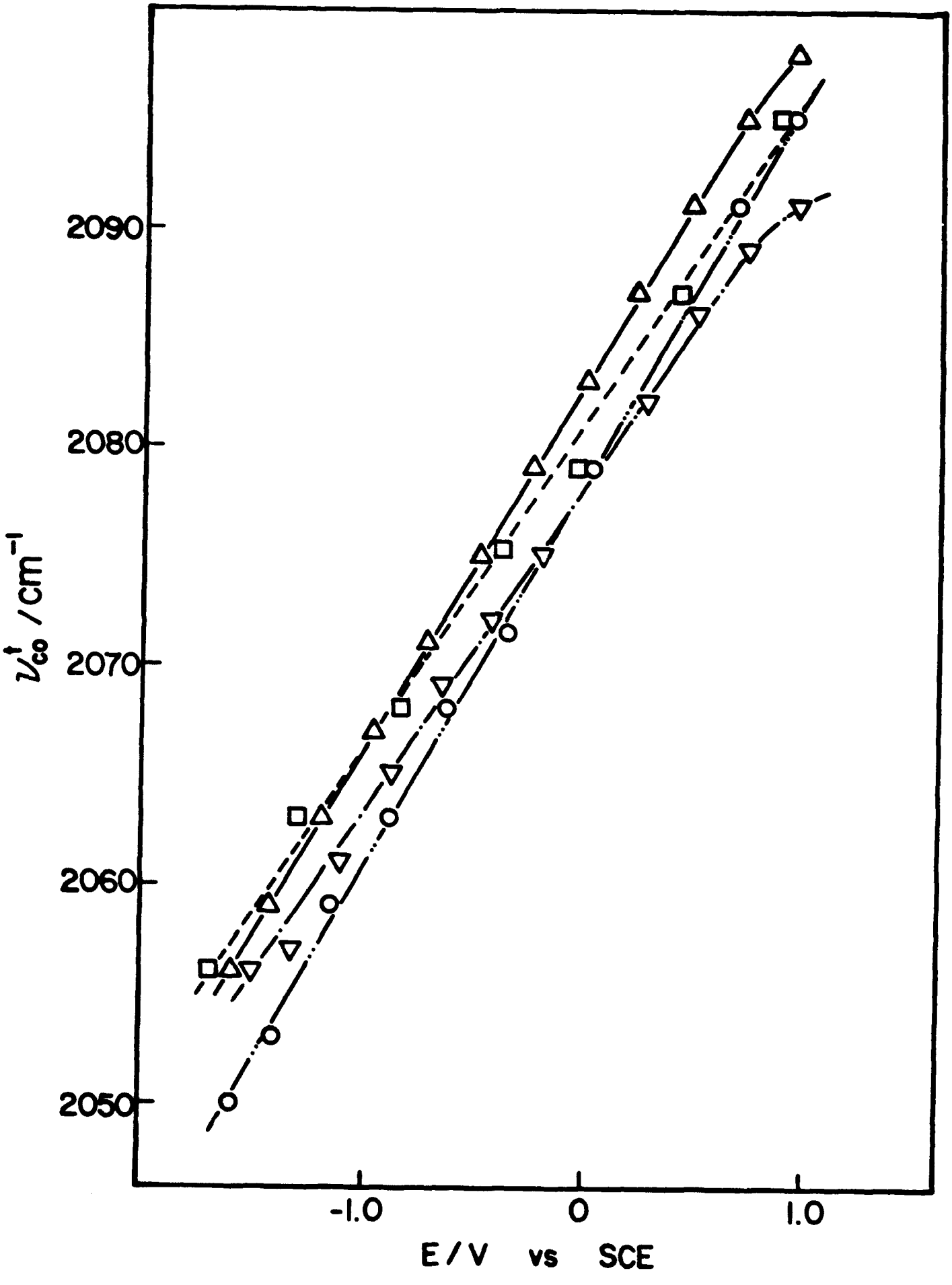

Fig. 2

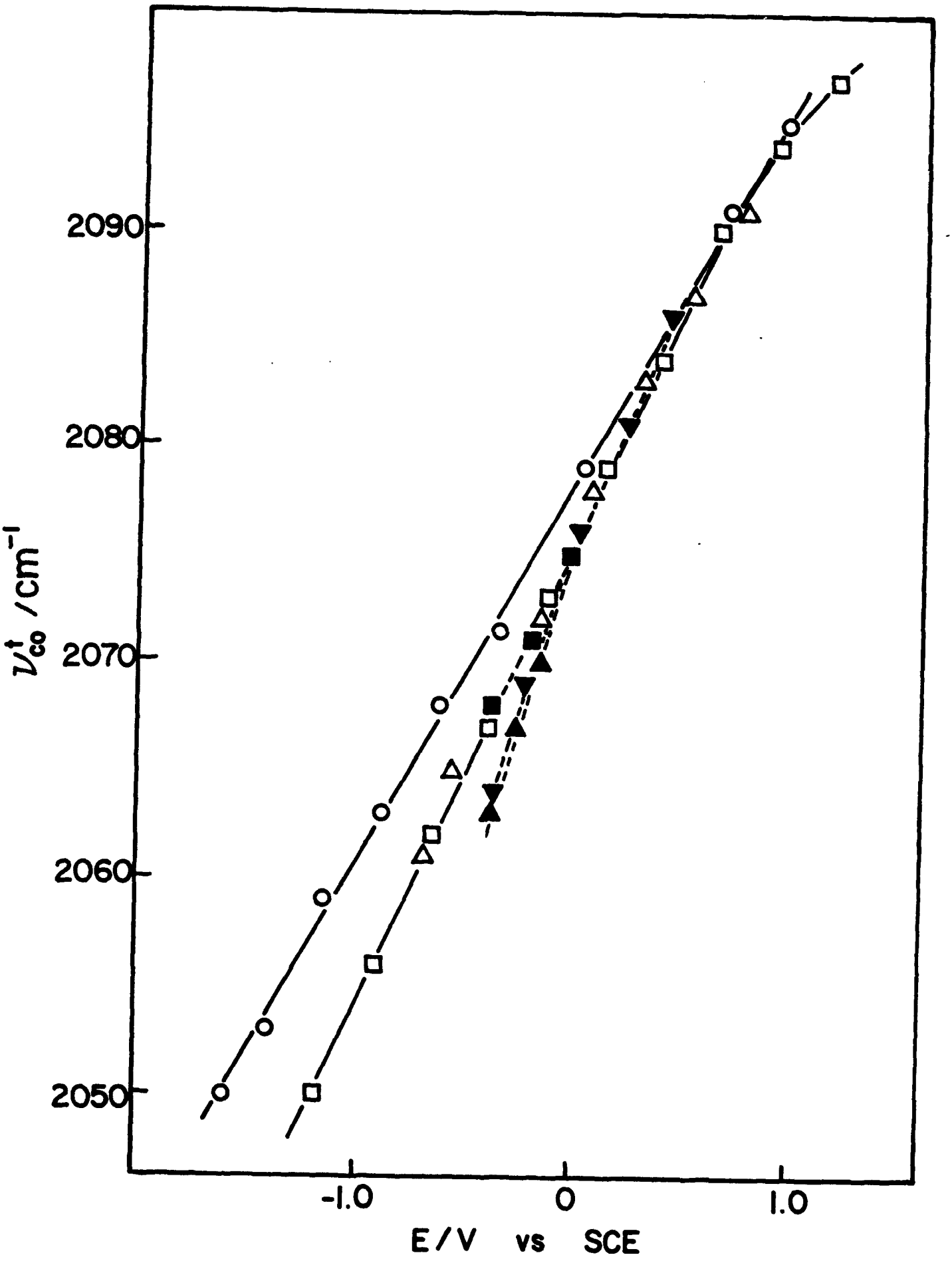

Fig. 3

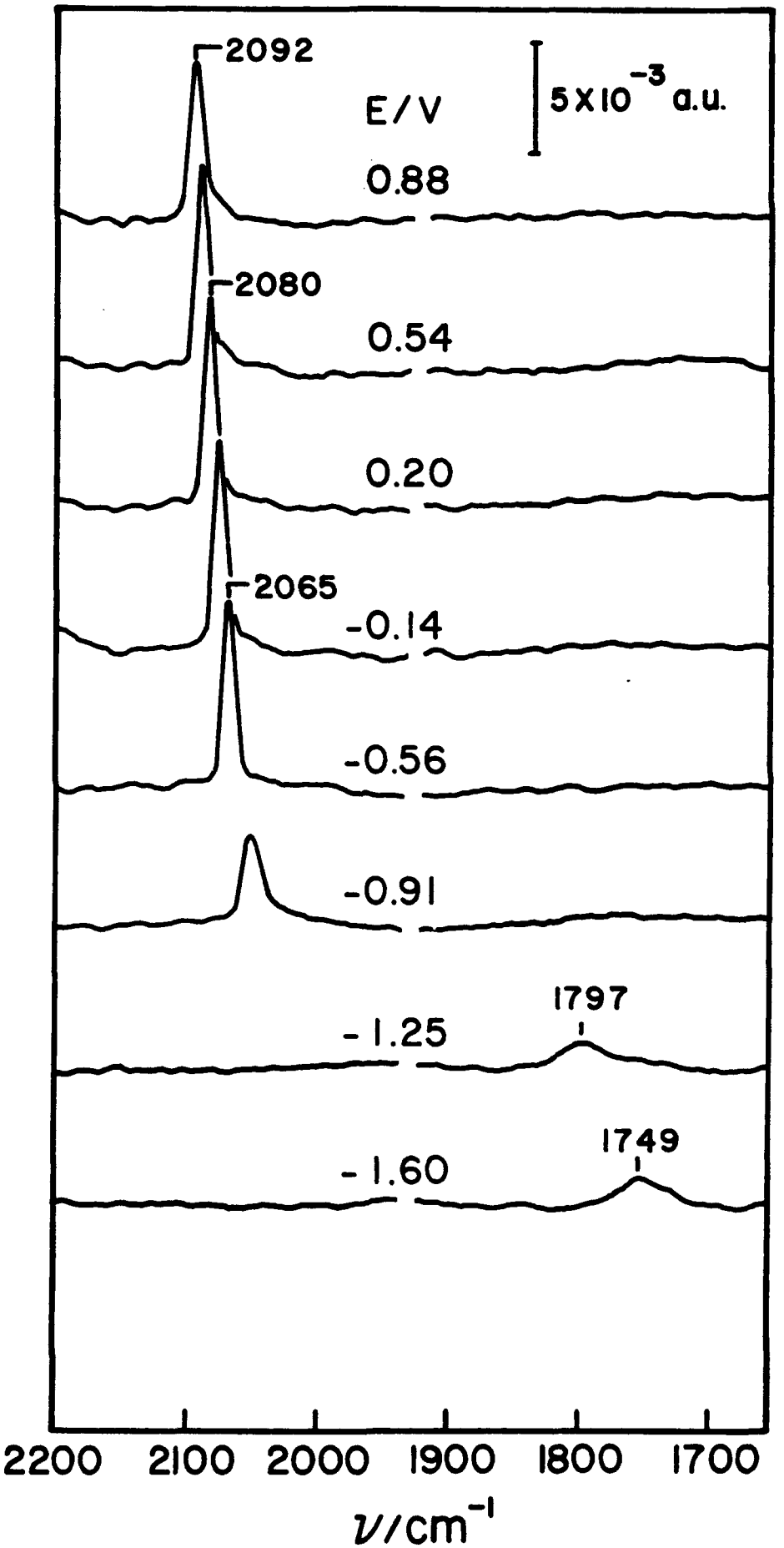
2092
E/V
5X10^-3 a.u.
0.88
2080
0.54
0.20
2065
-0.14
-0.56
-0.91
1797
-1.25
1749
-1.60
2200
2100
2000
1900
1800
1700
ν/cm^-1

Fig. 4

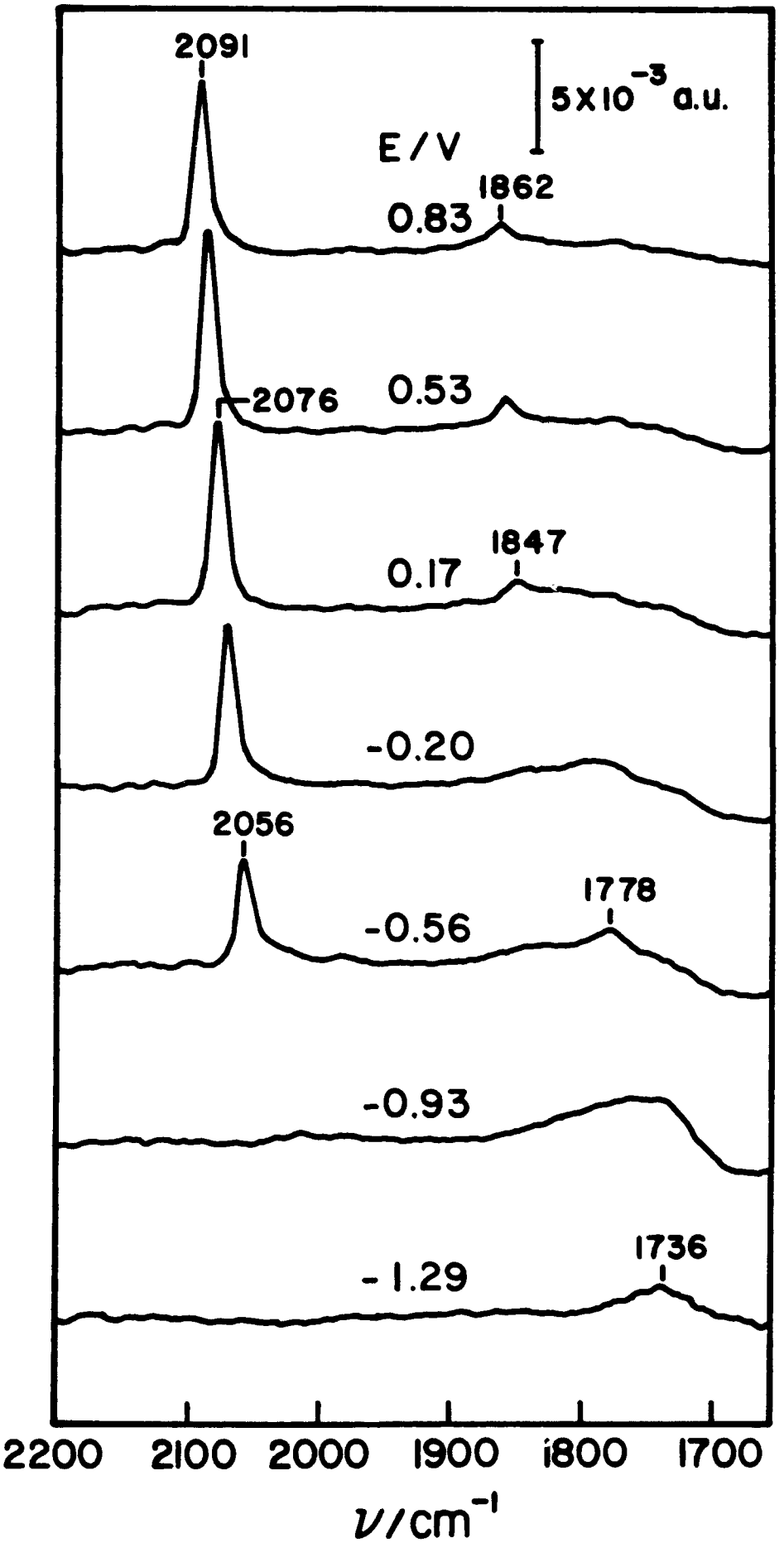
2091
5X10⁻³ a.u.
E/V
1862
0.83
2076
0.53
1847
0.17
-0.20
2056
1778
-0.56
-0.93
1736
-1.29
2200
2100
2000
1900
1800
1700
ν/cm⁻¹

Fig. 5

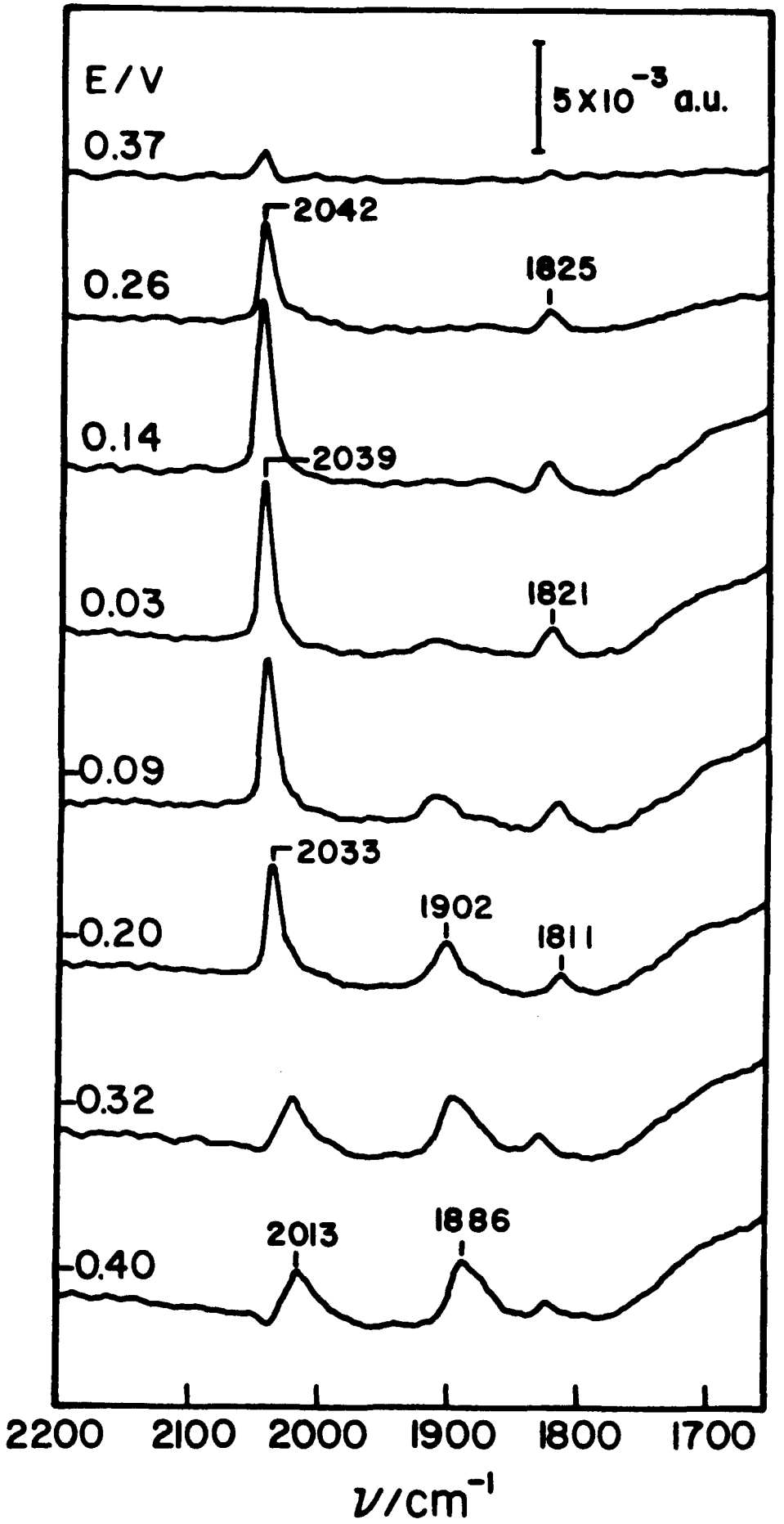
E/V
5X10⁻³ a.u.
0.37
2042
1825
0.26
0.14
2039
0.03
1821
0.09
2033
1902
0.20
1811
0.32
2013
1886
0.40
2200
2100
2000
1900
1800
1700
ν/cm⁻¹

Fig. 6

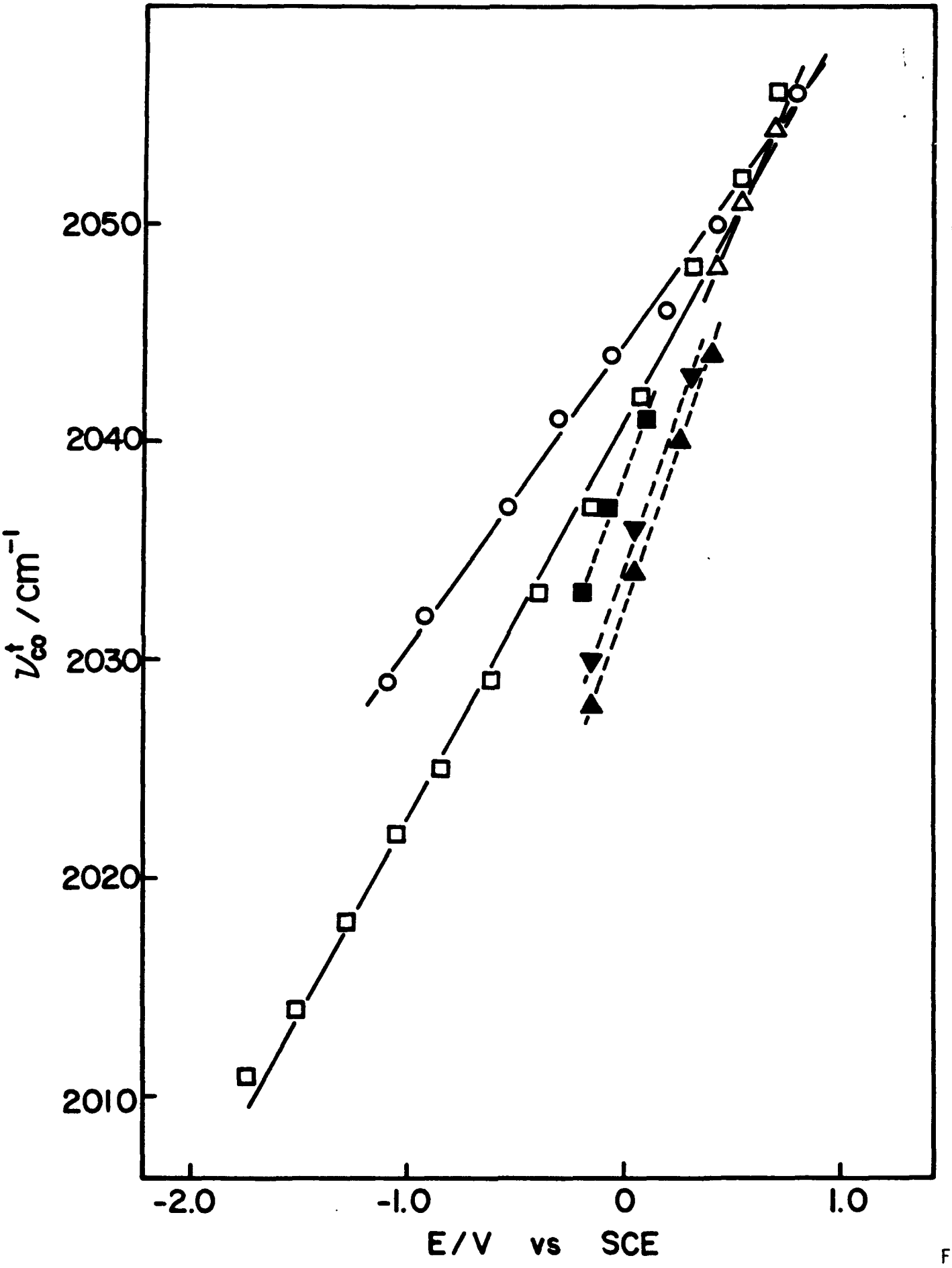

Fig. 7

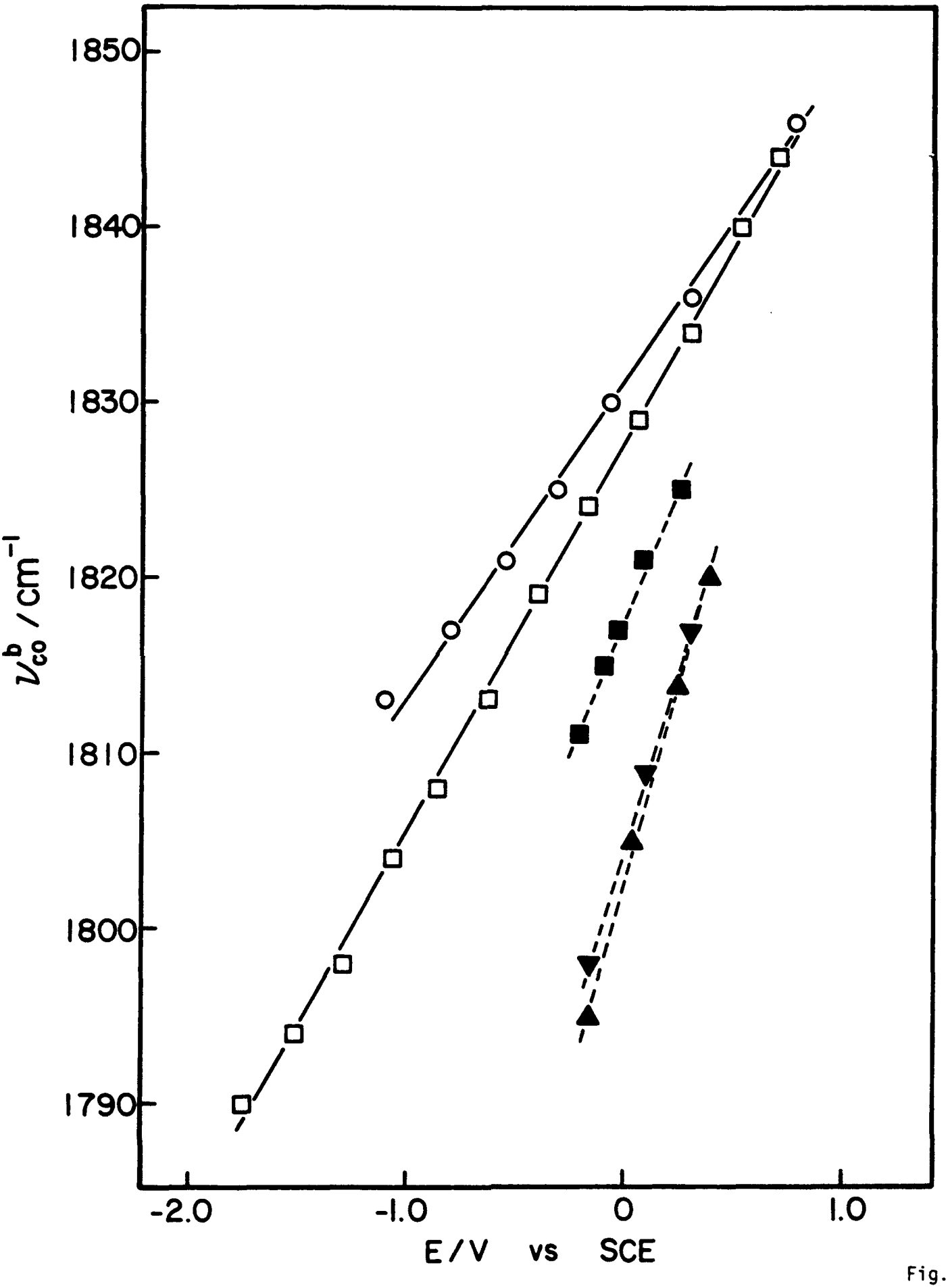
1850
1840
1830
1820
1810
1800
1790
ν_{CO}^{b} / cm^{-1}
-2.0
-1.0
0
1.0
E / V vs SCE

Fig. 8